TWO-DIMENSIONAL SOLAR MAPPING AT 5.2 CM WITH THE SIBERIAN SOLAR RADIO TELESCOPE

C. E. ALISSANDRAKIS

Section of Astrophysics, Astronomy and Mechanics, Department of Physics, University of Athens, GR-15784 Athens, Greece

B. I. LUBYSHEV, G. YA. SMOLKOV, B. B. KRISSINEL, T. A. TRESKOV, V. G. MILLER, and N. N. KARDAPOLOVA

Institute of Solar-Terrestrial Physics, 664033 Irkutsk 33, Russia

(Received 6 December, 1991; in revised form 27 April, 1992)

Abstract. We present two-dimensional solar maps at 5.2 cm computed from one-dimensinal observations with the Siberian Solar Radio Telescope (SSRT), using Earth rotation aperture synthesis techniques. The resolution attained with the E–W branch of the instrument is 15 by 45″ for a solar declination of about 23°. Maps during the period of June 8 to 13, 1988 clearly show the quiet-Sun background, sunspot and plage associated emission as well as compact sources above the neutral line in some active regions. We found that the latter disappear as the gradient of the longitudinal magnetic field decreases. We also detected emission associated with active regions behind the limb, apparently from unresolved loops, extending up to ~40″. The prospects of the SSRT, as a dedicated solar instrument, are discussed.

1. Introduction

The pursuit of high spatial resolution in the radio band has led to the construction of large instruments, such as the Westerbork Synthesis Radio Telescope (WSRT), the Very Large Array (VLA), and the RATAN-600. These instruments, designed primarily for celestial sources, have also been used for solar observations. This brought the spatial resolution of cm wavelength solar maps down to a few seconds of arc and opened up a new window in our study of the solar atmosphere (see, e.g., Kundu and Lang, 1985; Parijsky *et al.*, 1976).

The occasional use of large instruments for solar work does not permit the systematic study of solar phenomena in active regions and in the quiet Sun. The need for dedicated, high-resolution solar instruments led to the development of the Siberian Solar Radio Telescope (SSRT, Smolkov *et al.*, 1990; Smolkov, Treskov, and Potapov, 1986) and the Nobeyama Radioheliograph (Nakajima *et al.*, 1991), currently under construction.

Although, with the baseline increasing step by step, solar observations at the SSRT started in 1981 and new results have been obtained (Smolkov, Treskov, and Nefedjev, 1983; Zandanov, Treskov, and Uralov, 1983; Nefedjev *et al.*, 1988; Zubkova *et al.*, 1990; Lubyshev *et al.*, 1990; Maksimov *et al.*, 1991), the instrument has been used so far only for one-dimensional (fan-beam) observations of the Sun. In this paper we describe the use of the SSRT as a two-dimensional imaging instrument and we present some first results on active regions.

Solar Physics **142:** 341–358, 1992.

2. Instrumentation

The Siberian Solar Radio Telescope (Figure 1) is located at the Badary Station of the Radio Astrophysical Observatory of the Siberian Institute for Terrestrial Magnetism,

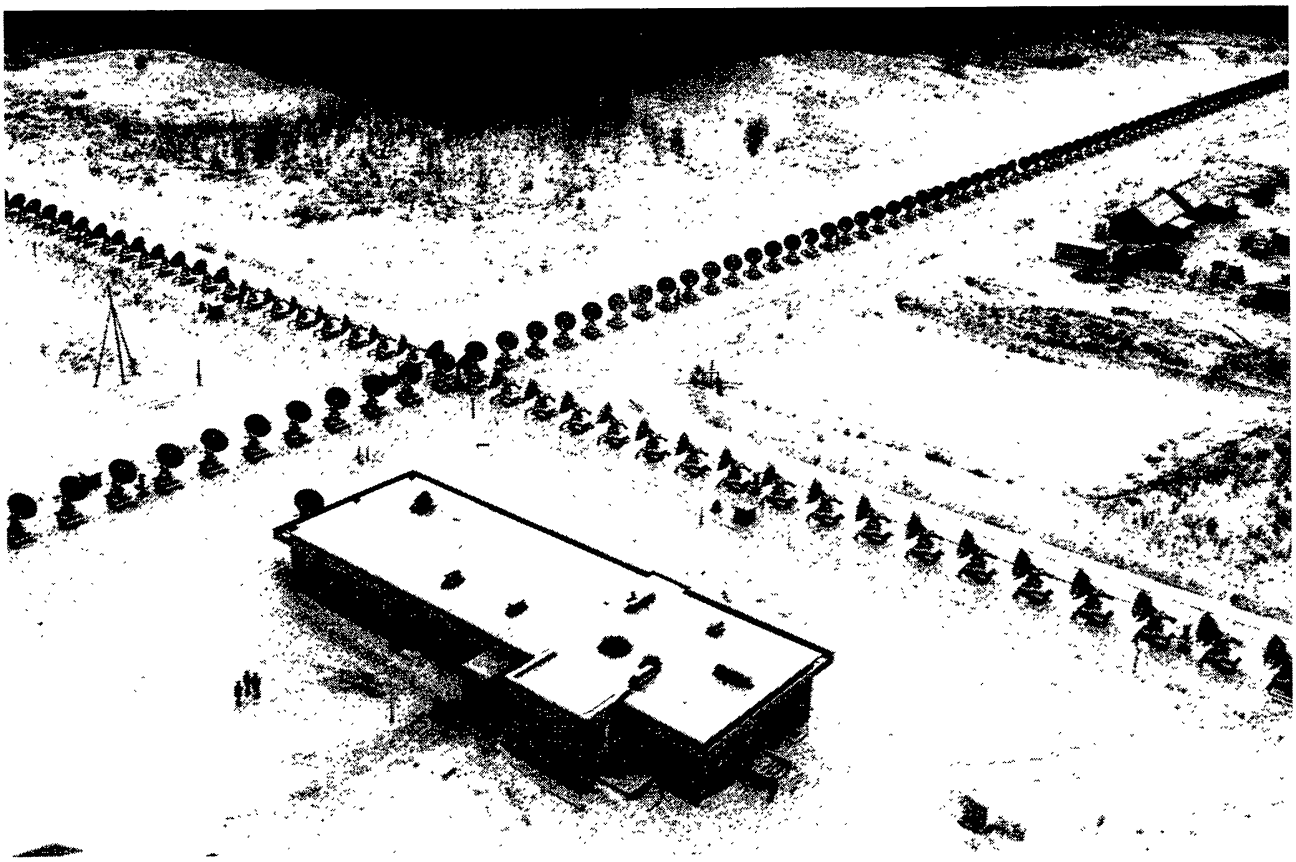

Fig. 1. A partial view of the Siberian Solar Radio Telescope. The E–W array extends from lower left to upper right.

the Ionosphere and Radio Wave Propagation (now Institute of Solar-Terrestrial Physics), 220 km south–west of Irkutsk, in the East Sayan Mountains (longitude $6^h48.9^m$ east, latitude 51°45.4′ north, altitude 832 m). In this and the next section we shall address only those instrumental questions which are associated with solar activity monitoring by linear arrays and the subsequent synthesis of radio images of active regions.

The SSRT is a cross instrument, with 128 antennas in the E–W direction and another 128 antennas in the N–S direction. At the time of writing all E–W antennas and 64 N–S antennas are operating, each array forming a separate linear interferometer. The beam pattern of each array is a set of knife-edge beams with fixed orientations; the individual antennas track the source, which is observed as it crosses the starionary fringes (beams) of the interferometers.

The instrument can operate in any of 180 frequency channels of 500 kHz bandwidth, in the range between 5675.241 and 5786.689 MHz (5.282 to 5.181 cm), with a frequency step of 622 kHz. In the usual operating mode a single frequency channel is used and

the one-dimensional intensity, as the Sun crosses the knife-edge beams, is digitized at a rate of one point per ~ 0.3 s and recorded on magnetic tape. In another observing mode, several closely spaced frequencies are used to provide a high temporal resolution, taking advantage of the fact that the knife beam position changes with the frequency of observation.

The antenna spacing is 4.9 m which provides a maximum baseline of 622.3 m (11967.3 λ at 5.2 cm); thus the E–W interferometer provides a maximum one-dimensional resolution of $\sim 17''$. Near the central meridian the Sun crosses the interferometer fringes every $2.43/\cos\delta$ min, wheren δ is the declination; this translates to a scan length (one-dimensional field of view) of $\sim 35'$, which is larger than the photospheric diameter. The length of the scan increases far from the central meridian. With all 128 antennas the resolution of the N–S array, in the N–S direction and near the central meridian, is $17''/\cos(\phi - \delta)$, where ϕ is the geographic latitude of the instrument; for a declination of 23° this gives a resolution of 19″ (38″ for 64 antennas). The diameter of the antennas is 2.5 m and thus the intensity at the solar limb is reduced by only 5% when the antennas are pointed at the center of the solar disk, making possible to map the entire Sun.

The noise temperature of the SSRT is determined by the feed system noise and by the noise of the integrated solar emission received by a single antenna. These noise temperatures are of the same order of magnitude. With a time constant of about 0.3 s, this corresponds to r.m.s. fluctuation of about 1% of the antenna temperature at one element, which makes it possible to record reliably fluxes down to 0.1 s.f.u.

Both Stokes parameters I and V are observed. The circular polarization in the SSRT is measured by means of modulation of the emission in the feed of each antenna. The polarization modulator is constructed by ferrite that rotates the plane of polarization by an angle of $\pm \pi/4$ and by a quarter-wave plate in front of it. The modulator is controlled by a square-shaped voltage. With such a design, a parasitic modulation from linear polarization arises due to modulator manufacturing errors and distortions in the modulating voltage. In view of the fact that, many years of observations made by a number of authors showed that the linear polarization in the S-component emission is very small, this error can be neglected. The parasitic modulation of the unpolarized signal, obtained from direct measurement, is less than 1%.

3. Data Reduction

The SSRT data are in the form of a set of one-dimensional scans, each produced as the Sun crosses the consecutive knife-edge beams of the interferometer. The change of the direction of the scans during the day makes possible the computation of two-dimensional maps, using aperture synthesis techniques. Aperture synthesis instruments, such as the VLA, observe directly the fringe visibility function, i.e., the Fourier transform of the image. Consequently the applicaiton of aperture synthesis in the SSRT data involves two additional steps: the separation of the scans out of the intensity-time record and the computation of their Fourier transform.

The absolute amplitude calibration and the correction for gain variations during the day was done by setting the flux of the Sun in each scan to the value published in *Solar Geophysical Data* (interpolated from Sagamore Hill observations at 8800 and 4995 MHz). The sky level was determined by computing the average value of the intensity at distances greater than 20′ from the disk center in scans far from the central meridian passage and subsequent linear interpolation.

Figure 2(a) shows the E–W data for June 9, 1988, after scan separation and gain

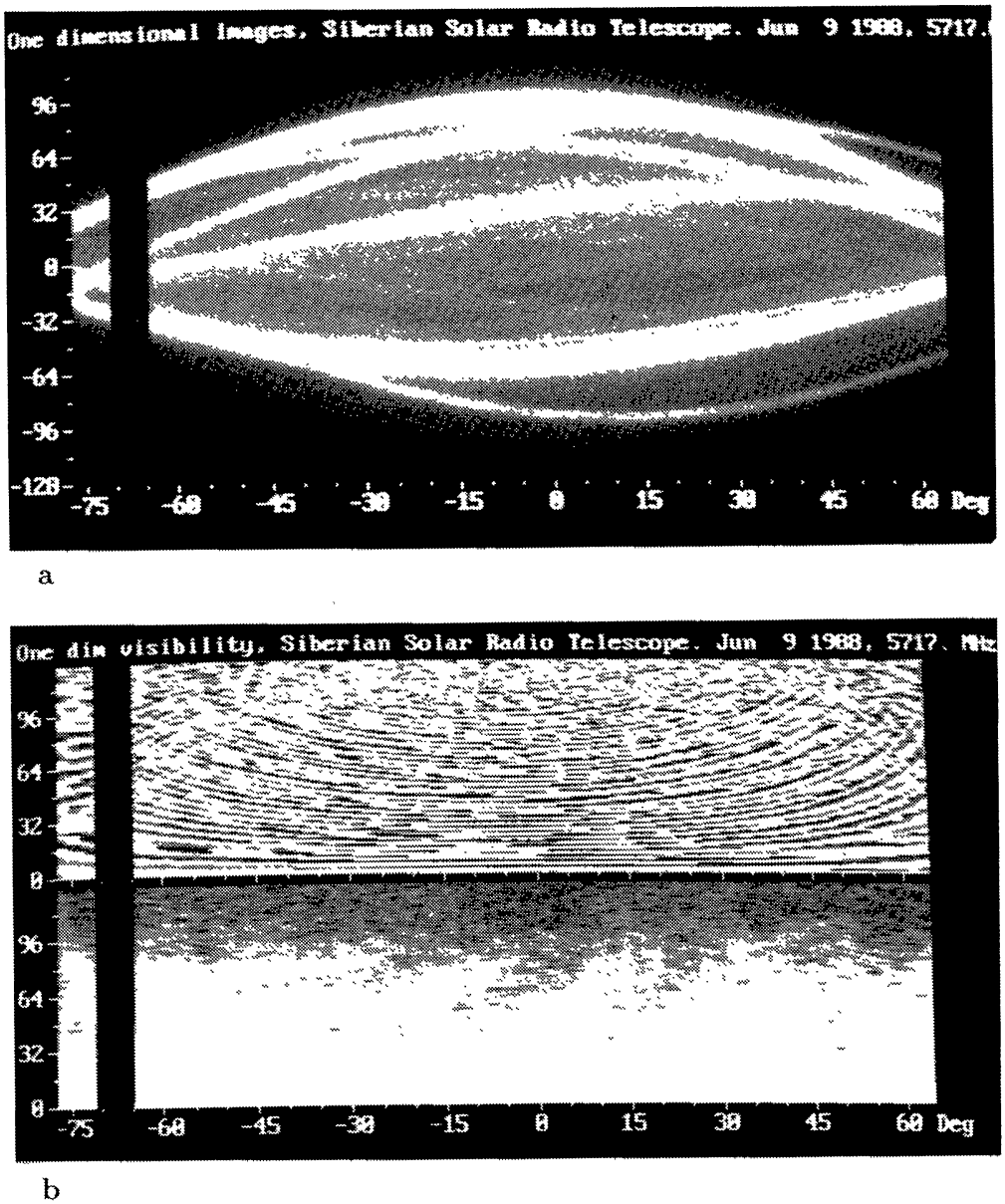

Fig. 2. (a) Gray scale representation of the one-dimensional intensity as a function of hour angle (abscissa, in degrees) and position. The position is given in units of 1/256 of the one-dimensional field of view and is positive towards the west; note that the field of view is smaller near central meridian passage and thus the quiet Sun appears larger there. (b) Visibility phase (*top*) and visibility amplitude (*bottom*) as a function of hour angle and baseline number (in units of the basic spacing of 4.9 m). The black region between $-65°$ and $-70°$ is a data gap.

correction, in the form of a gray scale representation of one-dimensional intensity as a function of hour angle (in degrees) and position. The 128 antennas of the array provide 128 baselines (including total power) and 256 independent data points for each scan; these are numbered from − 128 to 127 along the position axis of Figure 2(a). The length of the scan varies during the day, being shortest at central meridian passage; this effect changes the apparent size of the quiet Sun in the figure. On top of the quiet-Sun background several local sources can be seen in Figure 2(a). Their position changes with time, both due to the change of scan orientation during the day and because of the change of the true position scale.

Figure 2(b) shows the visibility phase (top) and amplitude (bottom) for the same day as a function of hour angle (in degrees) and baseline number (in units of the basic spacing of 4.9 m). The effects of noise show better at long baselines, where the solar signal is weaker; the fact that fringe patterns are visible up to the longest baselines in the phase display of Figure 2(b) indicates a low level of noise. This has been verified by plotting the visibility amplitude, averaged over all scans of the five observing days, as a function of baseline number (Figure 3); the plot shows a smooth, almost exponential decrease

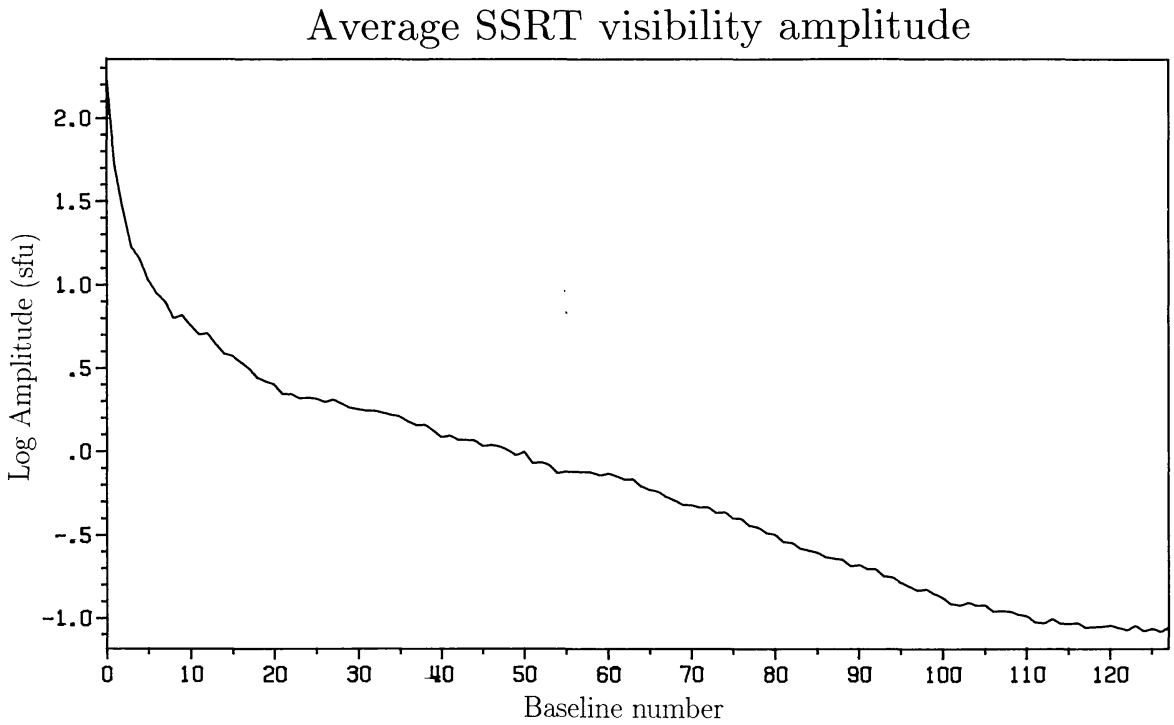

Fig. 3. Plot of the visibility amplitude, averaged over the entire observing period, as a function of baseline number for the E–W array.

of the amplitude up to baseline 115, with a subsequent flattening due to noise which is at the level of 0.1 s.f.u., in agreement with the discussion in Section 2. The same plot shows no apparent calibration problem in the relative amplitude of the baselines.

Once the visibility function has been computed, the calculation of two-dimensional maps is straightforward, provided that the sources do not change significantly during

the period of observation (cf. Kundu *et al.*, 1977). Here we followed a method similar to that used for the Nançay Radioheliograph (Alissandrakis, Lantos, and Nicolaidis, 1985): after elimination of scans affected by burst emission, the visibility is placed in a two-dimensional grid and it is Fourier transformed to give the 'dirty' map. The dirty map is subsequently decomposed to point sources using the 'CLEAN' method (Högbom, 1974) and then reconstituted assuming a gaussian beam.

The presence of the wide, high flux background component of the quiet Sun gives rise to a number of problems; it produces wide grating rings which are hard to separate from the principal images and makes CLEANing very difficult, since it is practically impossible to separate a very extended source into point-like sources. For the Nançay maps we have used a modelling technique: a model background source is computed from a least-square fit of the visibility, it is subtracted before the gridding stage and is added back to the clean map. Since at cm wavelengths the local sources are much brighter than the quiet-Sun background, we can simply ignore the shortest baselines where most of the quiet-Sun flux is (provided that we are interested in active regions only).

Due to a phasing problem in the N–S interferometer we only used E–W data for the maps presented in this paper. With only 64 antennas in operation the N–S resolution is 38″, while the N–S resoluton of a map computed using only the E–W array, with 12 hours of observations, is about 44″. Thus the N–S array at present does not improve significantly the resolution. In practice, however, the observations are shorter than 12 hours, thus the use of E–W data alone leaves gaps in the $u - v$ plane, with consequences primarily in the quiet-Sun background (see next section).

Due to solar rotation effects, it is impossible to compute a full resolution synthesis map of the entire Sun. Indeed, over 10 hours of observations a source at the center of the solar disk is displayed by 1.5′, which is much larger than the resolution of the instrument. Mapping of a moving source with a E–W array not only distorts its shape, but also displaces the source in the direction perpendicular to its motion. Therefore, for the computation of full disk maps we degraded the resolution to about 1′ and we corrected for rotation at a rate of 6.5° per day, which is half the solar rotation rate. Active region maps were computed separately, with the full resolution and the proper rotation correction in a limited field of view.

4. Results

4.1. Overall view

In this section we will present maps in total intensity (Stokes parameter I) and circular polarization (Stokes parameter V) for the period of June 8 to 11 and June 13, 1988. Figure 4 shows the full disk maps for June 9 and June 13, together with Ca II K_3 spectroheliograms from Meudon. The maps are normalized to the maximum intensity of each day and their resolution is degraded to 1′, for reasons explained in Section 3.

A comparison of the radio maps with the K_3 spectroheliograms shows that most of the emission comes from active regions, which will be described in more detail in the

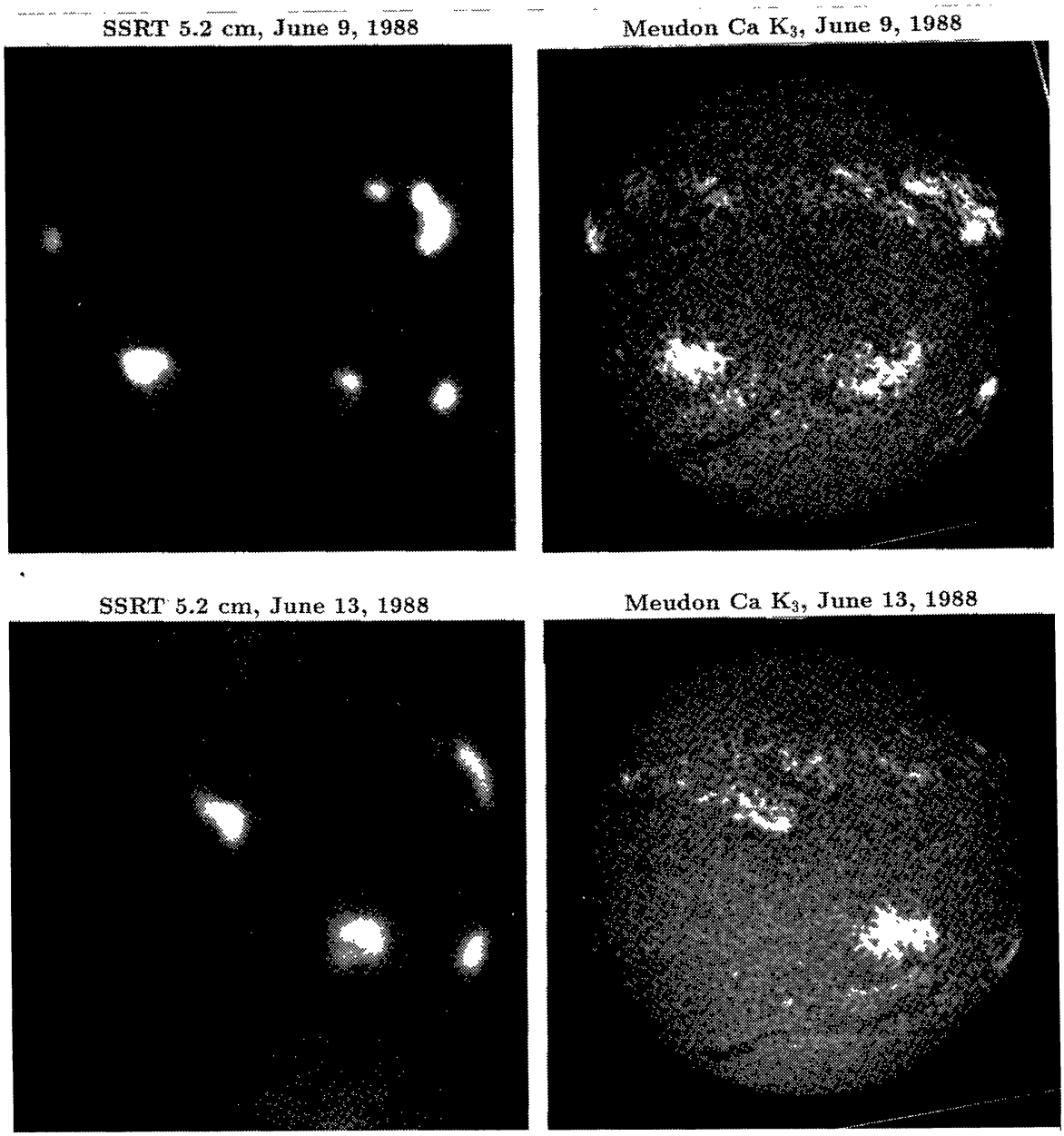

Fig. 4. Full-disk SSRT synthesis maps (*left*) and Meudon Ca K_3 spectroheliograms (*right*) for June 9 and June 13, 1988. The resolution of the radio maps has been degraded to 1′, to avoid distortion of the sources due to solar rotation; the maps are normalized to the peak brightness of each day, which on June 9 is about 2 times higher than on June 13. The photographs are oriented with the *solar* north up. On June 9 there are five active regions on the north hemisphere (NOAA numbers 5041, 5040, 5031, 5037, and 5032 from E to W) and three in the south (5036, 5034, and 5038). On June 13 the region 5041 is east and the region 5036 west of the central meridian. Approximately 10 hours of observations were used for the SSRT maps (average time ~05 : 10 UT); the K_3 images were obtained at 07 : 32 UT (June 9) and 09 : 26 UT (June 13).

next section. The active regions of June 9 can be identified on the scans of Figure 2(a), but their components are not resolved in the degraded two-dimensional map. Despite the fact that baselines shorter than ~150 λ were not used, the quiet Sun is still visible, in particular on June 13 when the local sources are weak; due to the lack of scans in the N–S direction the background shows up better in the E–W direction. The form of

the quiet-Sun emission is flat, with a diameter slightly larger than the photospheric diameter.

4.2. Active region 5036

This region was located at E 30 S 18 on June 9 (see Figure 4). High resolution (15″ by 47″) I and V maps are shown in Figure 5, together with Hα and Ca II K_1 spectroheliograms from Meudon as well as magnetograms from Kitt Peak. It is a very extended region, spanning more than 16° in longitude.

On June 8 the radio image consists of four discrete sources (labeled A to D, from E to W, in Figure 5), on top of a diffuse background. The sources are not fully resolved, their size being only slightly bigger than the beam; therefore the observed brightness temperatures are lower limits of the peak brightness temperature. A comparison with the K_1 photographs shows that source D is associated with the leading spot of the group, source A is associated with a trailing spot and source C is associated with an intermediate spot of the leading part of the group. The strongest source of the active region, B, with a peak observed brightness temperature of 7.5×10^5 K, is not associated with any particular spot; instead, it is located above the principal neutral line of the magnetic field and the active region filament. Similar high brightness sources have been observed above neutral lines by Alissandrakis and Kundu (1982) in WSRT observations at 6 cm and by Pulkovo group (Akhmedov *et al.*, 1986) in RATAN-600 observation in the range of 2 to 4 cm.

The same active region was observed by Raulin *et al.* (1991) at 21 and 92 cm with the VLA, but with an inferior resolution (27″ by 70″ at 21 cm). Their 21 cm map, around 14 : 00 UT of June 8, shows a diffuse source spanning the neutral line, with an E–W extent of about 4′; the peak was located slightly west of the neutral line, with a brightness temperature of 1.6×10^6 K. Raulin *et al.* observed the gradual appearance and disappearance of a weak second source in the western part of the region which may have triggered a noise storm. This event happened between 14 : 50 and 16 : 10 UT of June 8, which was after the end our observations; it left no apparent trace on the 5.2 cm emission.

All four sources are visible on the June 9 map. Their brightness is 10 to 20% lower, with the exception of the neutral line source, which decayed by about 40%. The K_1 data show some changes in the spots associated with sources A and C, while the leading spot, associated with source D, is fairly stable. The radio sources decay further during the next days: the neutral line source B as well as the source C disappeared on June 11 and only source D is still visible on June 13, with much reduced brightness (8.5×10^4 K). On the same day the diffuse background emission (halo component) is better visible, and it follows roughly the shape of the Hα plage.

The circular polarization maps reflect the polarity of the photospheric magnetic field only when the region is near the central meridian (June 10 and 11). During the other days the sense of circular polarization is affected by inversion and depolarization effects due to wave propagation (Cohen, 1960; Peterova and Akhmedov, 1973; Kundu *et al.*, 1977; Rjabov, 1981; Bandiera, 1982; Kundu and Alissandrakis, 1984). These effects can be

described in terms of the depolarization strip, which is the region around the line of zero circular polarization. On June 8 the depolarization strip falls on top of source *A*, which appears unpolarized. In the following days, as the region moves westwards, the depolarization strip is also displaced towards the west and the apparent polarization changes. Thus on June 9 the strip is located between sources *A* and *B*, on June 10 it is on the top of source *B* and on June 13 it is slightly eastwards of source *D* (note that the *V* observations were shorter on June 13 and therefore the quality of the map is inferior).

It is interesting to note that on June 8 the neutral line source is polarized. The polarization of a source in a region of transverse magnetic field should be linear and hence undetectable; however, propagation effects can change the linear polarization to right-hand circular, as observed.

4.3. Active region 5041

Figure 6 shows the observations of NOAA region 5041 on June 9, 10, and 13. On June 8 it was very close to the east limb; the associated 5.2 cm emission was weak, with some extension above the limb, apparently from active region loops. The optical data show that it is a developing active region with a large preceding spot of south magnetic polarity. Note that, due to projection effects, the magnetograms of June 9 and 10 do not reflect accurately the polarity of the vertical component of the magnetic field; in particular, the north polarity region (white in Figure 6) adjacent to the east side of the spot, is due to projection effects.

On June 9 and 10 the radio maps show two components. The strongest component (labeled *B* in Figure 6) is associated with the leading spot and the observed brightness temperature increased from 1.5×10^5 K on June 8 to 4.6×10^5 K on June 13. This is consistent with the growth of the photospheric magnetic field of the spot; during the same period the field increased from 2000 to 2800 G, according to *Solnechnye Dannye*, which implies that the gyroresonance layers moved higher, into hotter regions of the chromosphere–corona transition region. A weaker component (*A* in Figure 6) is visible, east of the strong component, from June 9 to 11. This component is no longer visible on June 13, when another weak component *D*, appared south–west of the main source; a second weak component, *C*, appeared on June 13 above the plage in the east part of the region.

A comparison of the radio source *A* with the K_1 photographs and the magnetograms on June 9 to 11 shows that it is not sunspot associated but it is located above the neutral line of the photospheric magnetic field. This is also true for the weak source *D* of June 13; its distance from the main source is considerably shorter than the distance of the large spot from the two small spots nearby. It is important to note that the disappearance of source *A* is apparently associated with the decrease of the gradient of the longitudinal magnetic field across that particular neutral line; this decrease is very obvious on the magnetograms, where on June 13 the two polarities are clearly separated everywhere along the neutral line except near the radio source *D*. As in the case of region 5036, the neutral line source *A* was circularly polarized on June 9 and 10 when, apparently, the depolarization strip was located east of the source.

1992SoPh..142..341A

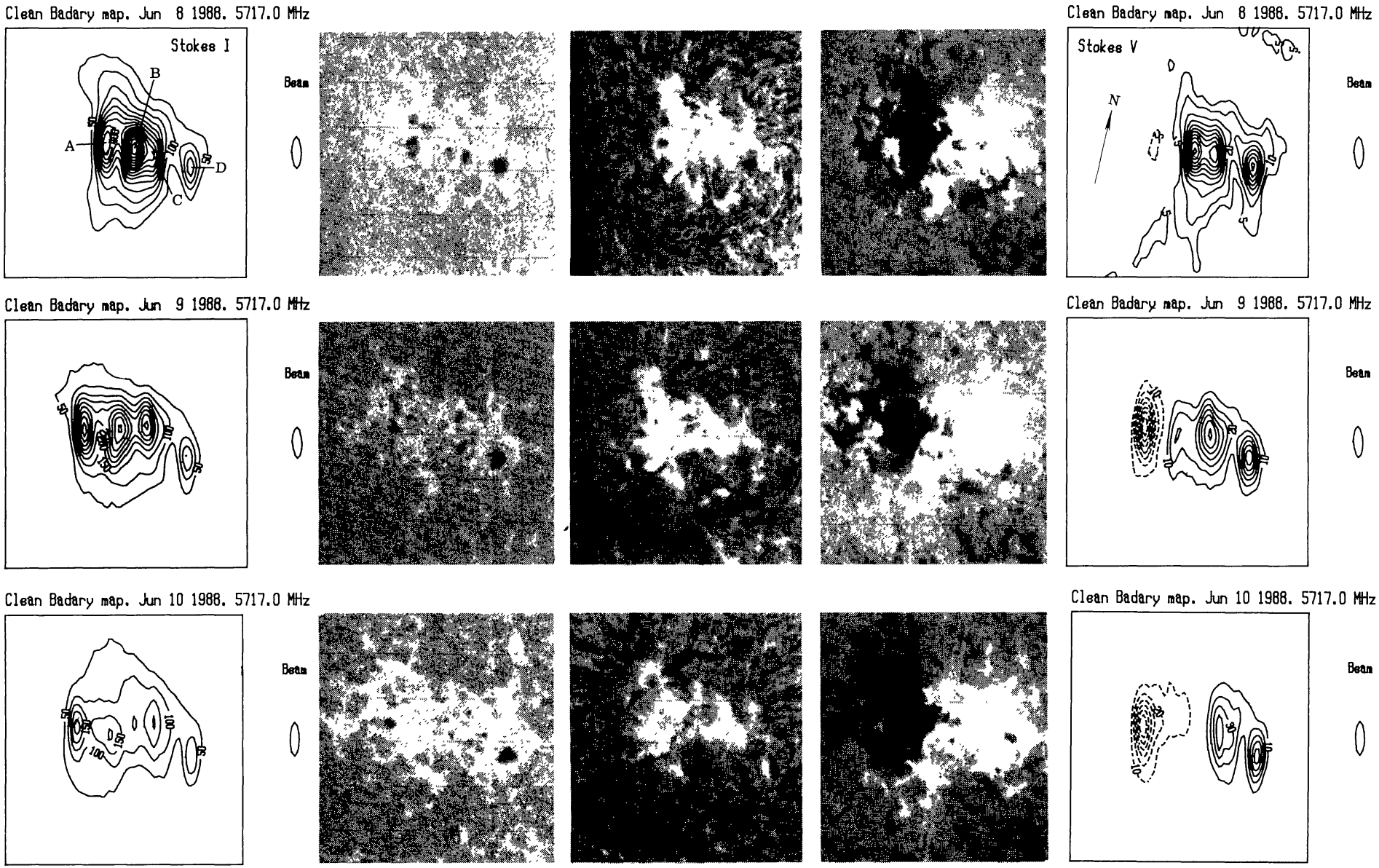

1992SoPh..142..341A

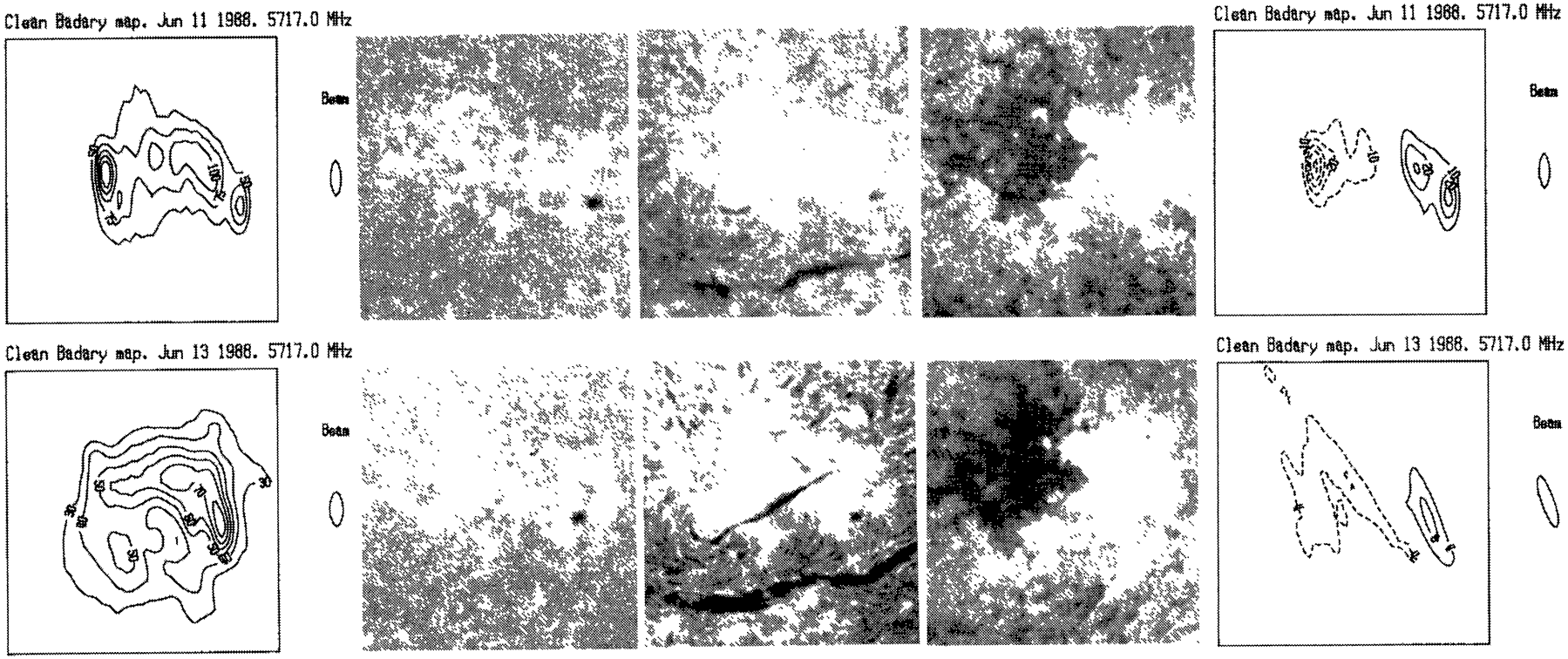

Fig. 5. High-resolution (15″ by 45″) SSRT maps of NOAA region 5036 in Stokes parameters I and V, together with Hα and Ca II K_1 spectroheliograms from Meudon and photospheric magnetograms from Kitt Peak. The field of view is 6′ by 6.3′. The average time of the SSRT maps is ~05 : 10 UT. The magnetograms were obtained at 15 : 43 UT (June 8), 13 : 26 UT (June 9), 14 : 41 UT (June 10), 13 : 32 UT (June 11), and 15 : 43 UT (June 13). The Hα photographs were obtained at 07 : 12, 07 : 27, 06 : 44, 12 : 12, and 06 : 36 UT, while the K_1 photographs were obtained at 07 : 26, 07 : 36, 07 : 20, 12 : 55, and 09 : 31 UT for June 8 to 11 and June 13, respectively. Contour labels are in 10^3 K. Dashed contours in the V maps indicate left-hand circular polarization. In this and subsequent figures the *celestial* north is up. The direction of the solar north is shown by the arrow on the V map of June 8.

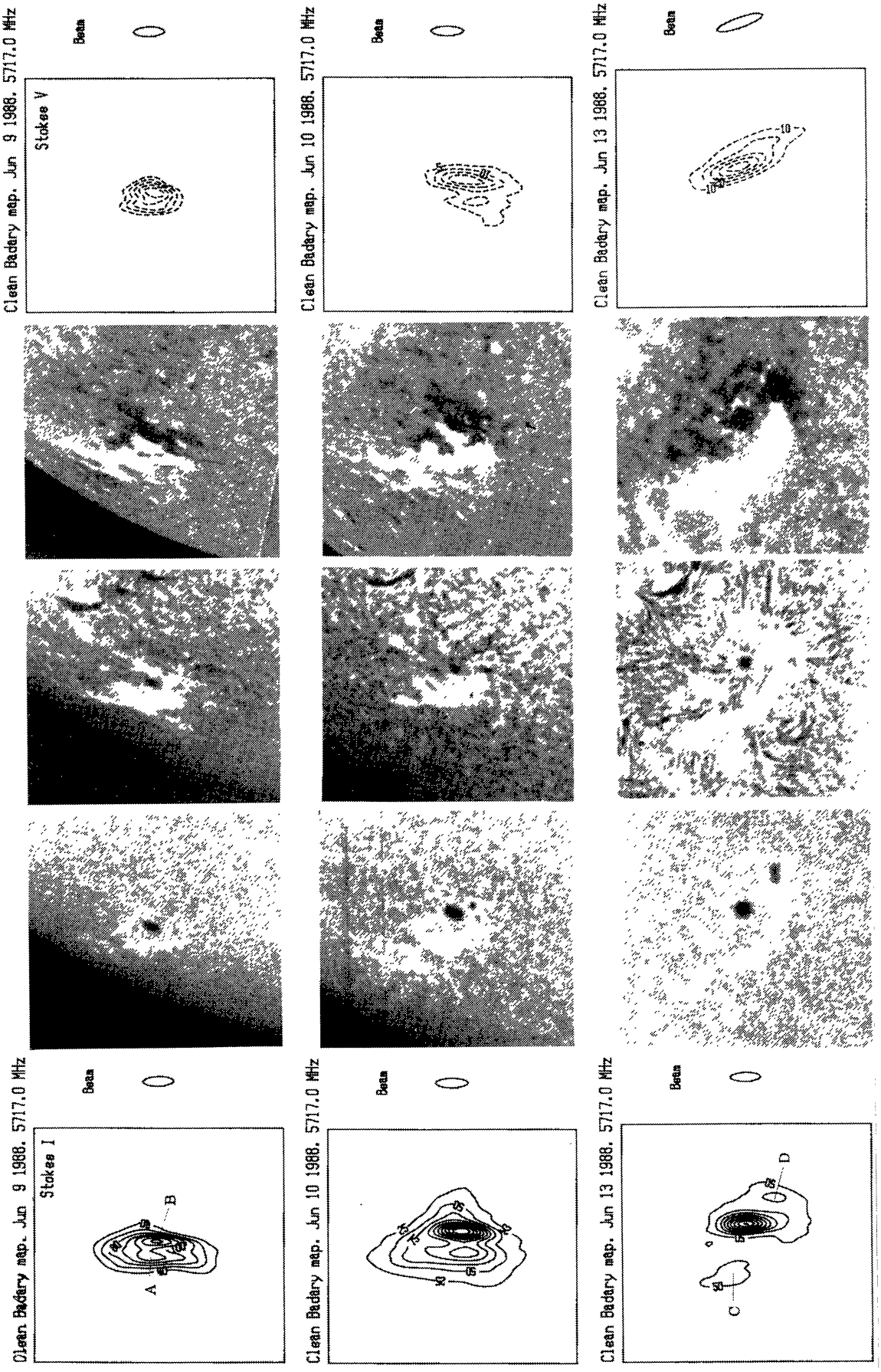

Fig. 6. Same as Figure 5 for NOAA region 5041 on June 9, 10, and 13. The field of view is 6′ by 6.3′.

4.4. Other regions

During our period of observations the solar disk was rich in active regions. For the sake of conciseness we will only present selected maps here. Figure 7 shows a complex of four active regions, NOAA numbers 5040, 5031, 5037, and 5032, which were located on the north–west quadrant of the disk on June 9 (cf. Figure 4). The strongest radio emission ($T_b = 9.1 \times 10^5$ K) comes from the main spot of region 5031 which, according to *Solnechnye Dannye*, had a peak magnetic field of 3600 G. The V map shows a double-peaked source, similar to the one observed by Kundu *et al.* (1977) and interpreted by Alissandrakis, Kundu, and Lantos (1980) in terms of the convolution of a ring-shaped source with the instrumental beam; the ring shape of the V source reflects the larger size of the *e*-mode emission (which originates in the third harmonic layer), compared to that of the *o*-mode (which comes primarily form the second harmonic layer).

The trailing part of region 5031 is located quite far from the leading part, and it is in contact with the leading part of active region 5040 (cf. magnetograms in Figure 7); sunspot drawings from *Solar Geophysical Data* show that the region 5040 emerged on June 8, in the trailing pat of the old region 5031. In the radio maps, the region 5040 and the trailing pat of region 5031 appear as a single source with three sunspot-associated components, each polarized in the sense of the extraordinary mode of the photospheric magnetic field.

The radio image of region 5037 shows two components, associated with small spots; the sense of polarization of the limbward component is inverted due to wave propagation effects. It is interesting to note that, although the leading part of region 5031 is closer to the limb than 5037, no polarization inversion is observed there. This is due to the fact that the magnetic structure in region 5037 is much more compact. Finally the region 5032 does not show up as a discrete radio source, but rather as a local enhancement of the radio emission.

The other two active regions observed on June 8 are shown in Figures 8 and 9. Both were located in the south hemisphere. Region 5034 (Figure 8) is a decaying active region with an extended plage; the radio map shows a sunspot associated component with a brightness temperature of 4×10^5 K, polarized in the extraordinary sense. Region 5037 (Figure 9) shows two distinct sources, corresponding to leading and trailing spots; they are both polarized in the same sense due to the inversion of the polarization of the limbward source.

In the course of our observations some sources appeared from behind the east limb while others disappeared behind the west limb. In Figure 10 we present a rising and a setting source; such observations are interesting because they provide information on the vertical extent of the emission. The rising source (left side of Figure 10) is the NOAA region 5047, the first sunspot of which appeared on June 14, one day after the radio map; note also that there is practically no trace of plage on the K_3 photograph in Figure 4. It is obvious from the figure that the emission comes from behind the limb, apparently from unresolved loops extending up to about 40″ above the limb as seen at

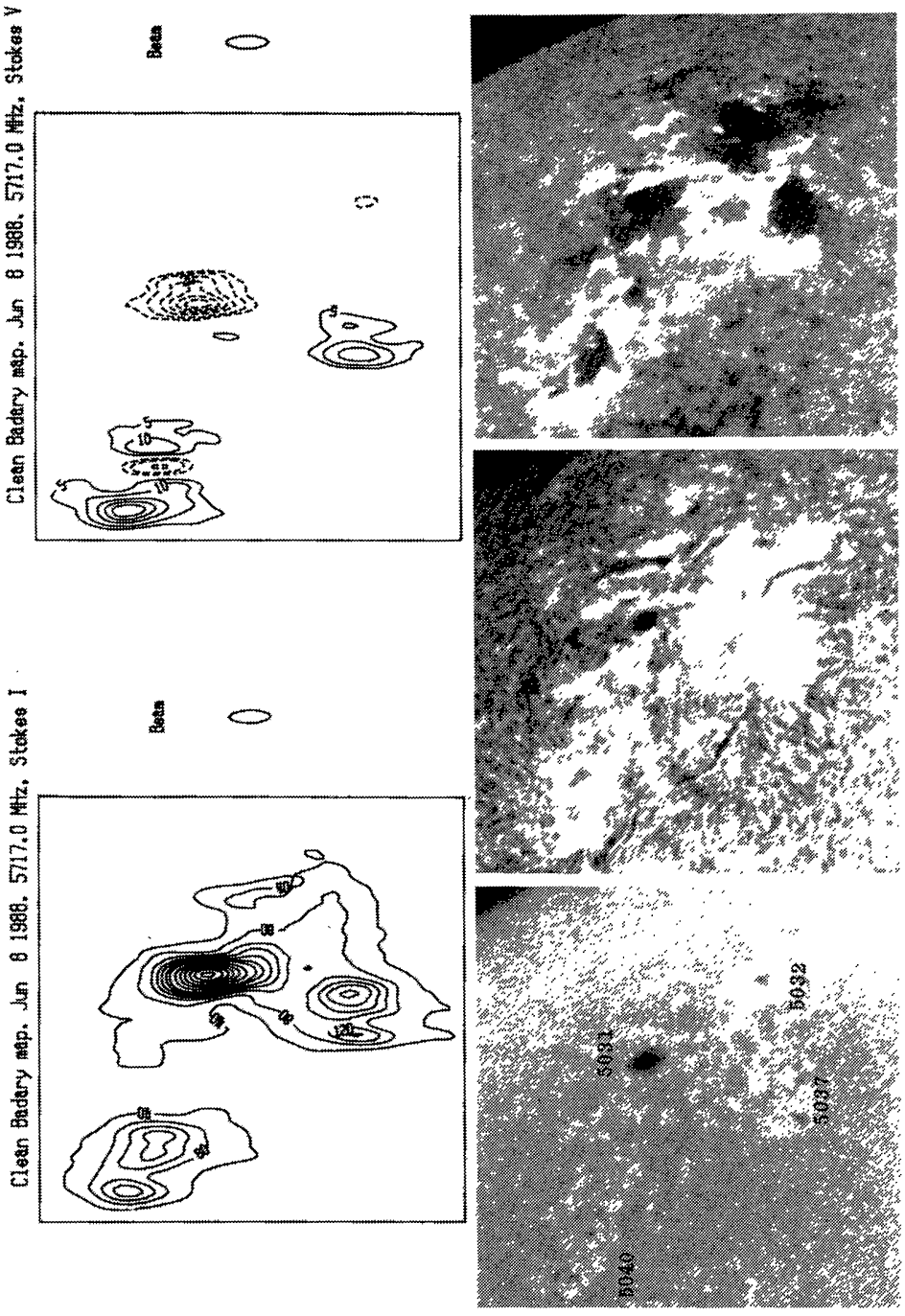

Fig. 7. Observations of NOAA regions 5040, 5031, 5037, and 5032 on June 8, 1988. The field of view is 8′ by 9′.

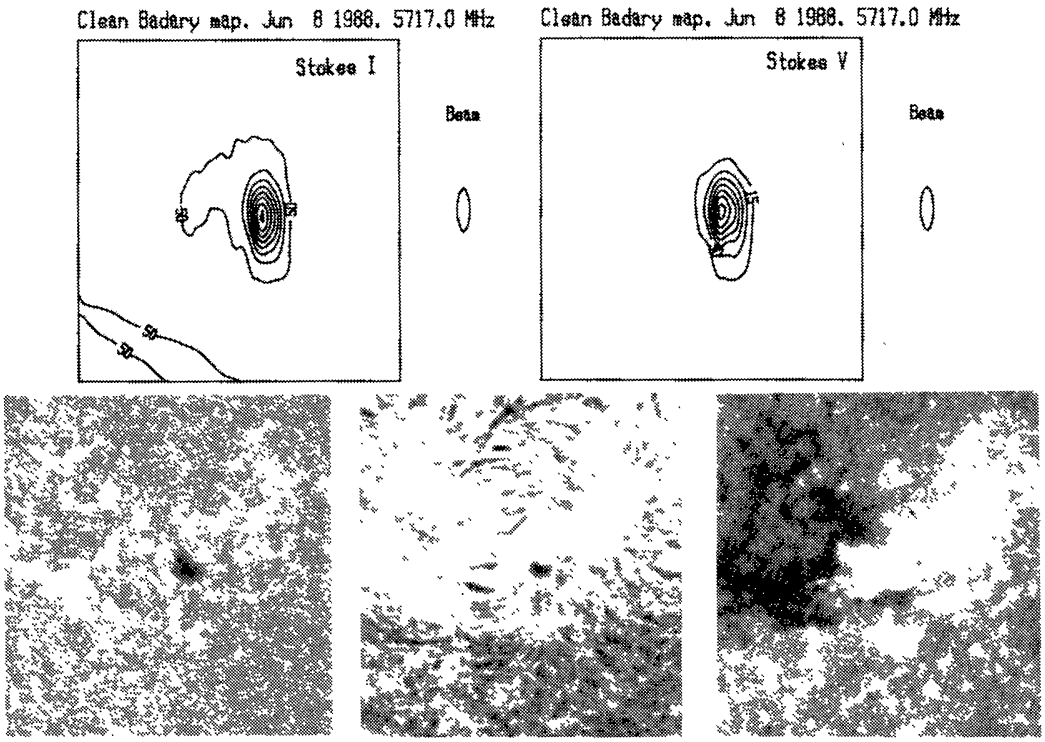

Fig. 8. The NOAA region 5034 on June 8, 1988. The field of view is 6′ by 6.3′.

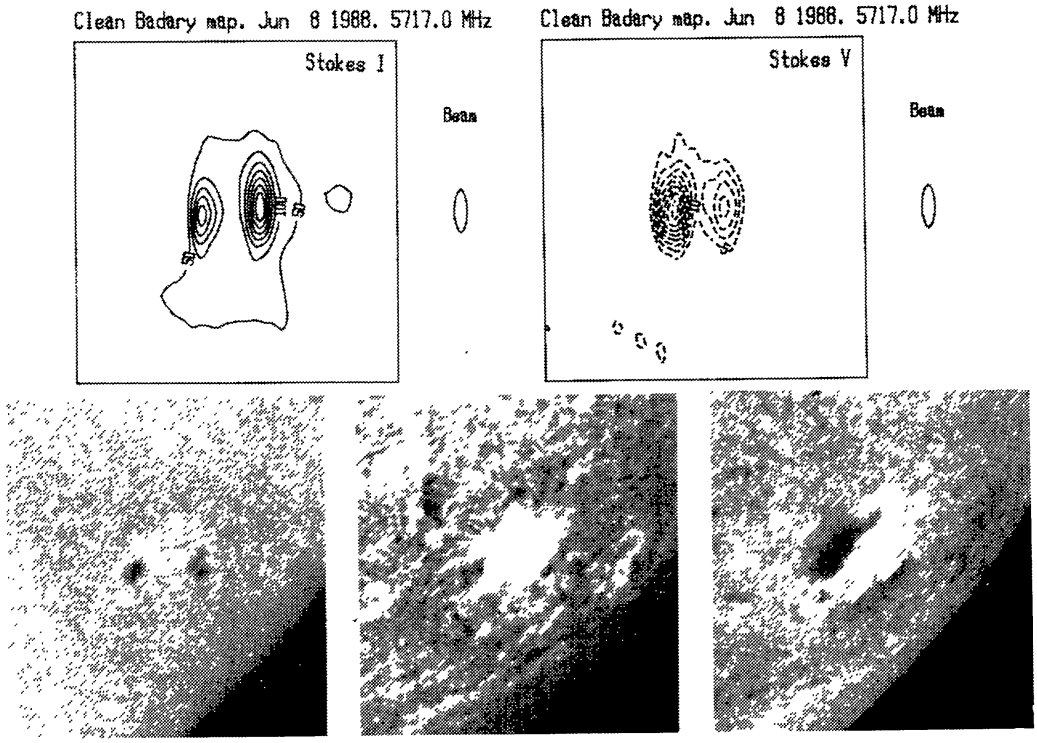

Fig. 9. The NOAA region 5038 on June 8, 1988. The field of view is 6′ by 6.3′.

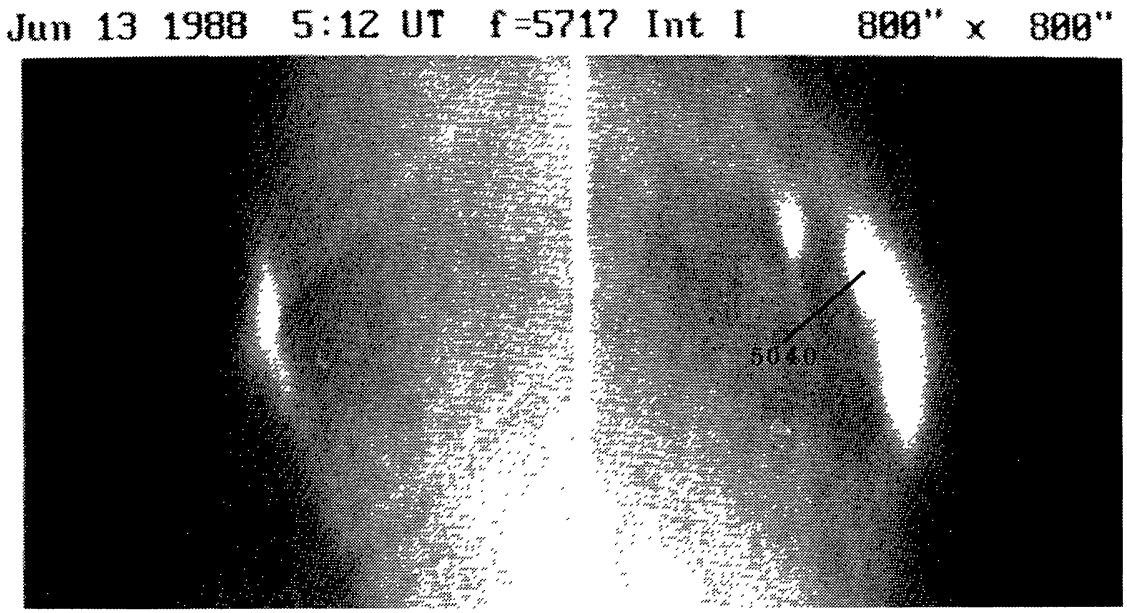

Fig. 10. Emission from active regions near and behind the east (left) and the west (right) limb on June 13, 1988.

5.2 cm. The same figure shows that the 5.2 cm limb, seen with a resolution of 15″, is fairly sharp.

The setting source in Figure 10 (right part) is the region 5040 which was very close to the west limb, while the other regions of the complex discussed in the beginning of this section (lower part of the figure) were already behind the limb (cf. again with the K_3 photograph in Figure 4); in spite of that, some emission is still present, with a peak brightness temperature of 6.5×10^4 K above the quiet-Sun level, extending about 30″ above the limb. The limited extent of the emission of region 5040, which is about equal to the instrumental beam, shows that the sunspot-associated component is very flat.

5. Summary and Discussion

The two-dimensional maps obtained with the SSRT have been used in the study of the structure and evolution of solar active regions at 5.2 cm. Sunspot-associated sources were not fully resolved with the present resolution of 15″ by 45″ and their observed brightness temperature ranged from 0.5 to 0.9×10^6 K. Active regions behind the limb show weak emission extending up to about 40″ above the sharp radio limb, apparently from coronal loops.

We detected neutral line sources (NLS) in two active regions. Whereas the cm wavelength emission from sunspot associated sources is well understood in terms of thermal gyroresonance (Zheleznyakov, 1970; Alissandrakis, Kundu, and Lantos, 1980), the origin of intense emission above neutral lines of the magnetic field is still an open question. Kundu and Alissandrakis (1984) pointed out their association with emerging flux and with high gradient of the magnetic field. Both of these characteristics are

confirmed by the data presented here. In particular, the NLS disappeared when the longitudinal field gradient became too small, while their locations coincided with areas where new pores formed. It is interesting, however, to point out that one NLS appeared in a decaying region (NOAA 5036, Section 4.2).

The evolution of neutral line sources (NLS), to which a large part of this paper has been devoted, is a good example of what can be done with the SSRT. Such sources have been reported in the literature but have not been studied in detail. The long-term evolution of sunspot-associated sources is another subject where the SSRT can provide an important contribution. Although its resolution is not sufficient for studying the fine structure of such sources, it can tackle interesting problems, such as the presence of low temperature material in the corona above sunspots (cf. Alissandrakis and Kundu, 1982). The large-scale structure of the active region magnetic field can be studied from observations of the inversion of the circular polarization due to wave propagation effects. Last but not least, the fact that the dynamic range and the $u - v$ coverage of the instrument are sufficient to show the solar disk under conditions of high activity, proves that the instrument will be appropriate for quiet-Sun studies in periods of low activity.

The SSRT has been designed and constructed as a dedicated solar instrument, which makes it suitable for systematic studies of solar phenomena. The development of two-dimensional mapping from the one-dimensional data is an essential step in this direction. In the very near future it is planned to conduct observations with the SSRT in the crossed mode. The crossed mode will provide several tens of two-dimensional full disk maps of the Sun per day, with an angular resolution of $\sim 20''$; thus, in addition to the higher spatial resolution, the temporal resolution will improve substantially and will permit the investigation of discrete components of active region emission.

Acknowledgements

We wish to thank Dr B. Schmieder of Meudon for providing the spectroheliograms and the Kitt Peak National Observatory for the magnetograms used in this publication. This work has been supported in part through the Greek–Soviet bilateral agreement on scientific and technical collaboration.

References

Akhmedov, Sh. B., Borovik, V. N., Gelfreikh, G. B., Bogod, V. M., Korzhavin, A. N., Petrov, Z. E., Dikij, V. N., Lang, K. R., and Willson, R. F.: 1986, *Astrophys. J.* **301**, 460.
Alissandrakis, C. E. and Kundu, M. R.: 1982, *Astrophys. J.* **253**, L49.
Alissandrakis, C. E., Kundu, M. R., and Lantos, P.: 1980, *Astron. Astrophys.* **82**, 30.
Alissandrakis, C. E., Lantos, P., and Nicolaidis, E.: 1985, *Solar Phys.* **97**, 267.
Bandiera, R.: 1982, *Astron. Astrophys.* **112**, 52.
Cohen, M. H.: 1960, *Astrophys. J.* **131**, 664.
Högbom, J. A.: 1974, *Astron. Astrophys. Suppl.* **15**, 417.
Kundu, M. R. and Alissandrakis, C. E.: 1984, *Solar Phys.* **94**, 249.
Kundu, M. R. and Lang, K.: 1985, *Science* **228**, 9.
Kundu, M. R., Alissandrakis, C. E., Bregman, J. D., and Hin, A. C.: 1977, *Astrophys. J.* **213**, 278.

Lubyshev, B. I., Agalakov, B. V., Nasonova, O. N., Smolkov, G. Ya., and Treskov, T. A.: 1991, *Issled. Geomagn. Aeron. Fiz. Sol.* **95**, 166.

Maksimov, V. P., Nefedjev, V. P., Smolkov, G. Ya., and Bakunina, I. A.: 1991, in R. Thompson (ed.), *Proceedings of the Leura STP Workshop* (in press).

Nakajima, H. and the Radioheliograph Group: 1991, in *Symposium on the Nobeyama Radioheliograph,* p. 3.

Nefedjev, V. P., Korobova, Z. B., Smolkov, G. Ya., and Urpo, S.: 1988, in *Finish–Soviet Symposium on Radio Astronomy*, University of Turku, p. 38.

Parijsky, Yu. N., Korolkov, D. V., Shivris, O. N., Kajdanovskij, N. L., Esepkina, N. A., Zverev, Yu. K., Stotckij, A. A., Akhmedov, Sh. B., Bogod, V. M., Boldyrev, S. I., Gelfreikh, G. B., Ipatova, I. A., Korzhavin, A. N., and Romantzov, V. V.: 1976, *Astron. Zh.* **53**, 1017 (*Soviet Astron.* **20**, 577).

Peterova, N. G. and Akhmedov, Sh. B.: 1973, *Astron. Zh.* **50**, 1220 (*Soviet Astron.* **17**, 768).

Raulin, J. P., Wilson, R. F., Kerdraon, A., Klein, K.-L., Lang, K. R., and Trottet, G.: 1991, *Astron. Astrophys.* **251**, 298.

Rjabov, B. I.: 1981, *Issled. Sol. Krasn. Zvezd* **15**, 5.

Smolkov, G. Ya., Treskov, T. A., and Nefedjev, V. N.: 1983, *Sol. Aktiv.,* Nauka, Alma-Ata, p. 54.

Smolkov, G. Ya., Treskov, T. A., and Potapov, N. N.: 1986, *Issled. Geomagn. Aeron. Fiz. Sol.* **65**, 204.

Smolkov, G. Ya., Pistolkors, A. A., Treskov, T. A., Krissinel, B. B., Putilov, V. A., and Potapov, N. N.: 1986, *Astrophys. Space Sci.* **119**, 1.

Smolkov, G. Ya., Krissinel, B. B., Treskov, T. A., Potapov, N. N., and Miller, V. G.: 1990, *Issled. Geomagn. Aeron. Fiz. Sol.* **91**, 146.

Zandanov, V. G., Treskov, T. A., and Uralov, A. M.: 1983, *Issled. Geomagn. Aeron. Fiz. Sol.* **68**, 21.

Zheleznyakov, V. V.: 1970, *Radio Emission of the Sun and Planets,* Pergamon Press, Oxford.

Zubkova, G. N., Kardapolova, N. N., Lubyshev, B. I., Nefedjev, V. P., Smolkov, G. Ya., Sych, R. A., and Treskov, T. A.: 1990, *Astron. Nachr.* **311**, 313.